Available online at www.sciencedirect.com
SCIENCE DIRECT
Polymer 46 (2005) 7386–7393
polymer
www.elsevier.com/locate/polymer

Vibrational dynamics and heat capacity in syndiotactic poly(propylene) form II

Vikal Saxena, Radha Mohan Misra, Poonam Tandon*, Vishwambhar Dayal Gupta

Physics Department, Lucknow University, University Road, Lucknow, Uttar Pradesh 226 007, India

Received 21 December 2004; received in revised form 11 June 2005; accepted 14 June 2005
Available online 14 July 2005

Abstract

Normal modes and their dispersion are obtained for planar-zigzag form II (*tttt*) of syndiotactic polypropylene (sPP) in the reduced zone scheme using Urey–Bradley force field and Wilson's GF matrix method as modified by Higgs. It is observed that this all *trans* backbone conformation can be characteristized by a band at 1233 cm^{-1} (calculated at 1239 cm^{-1}). A comparison is made with the spectra of its isotactic and helical form. Characteristic features of the dispersion curves such as crossing, repulsion and von Hove type singularities (regions of high density-of-states) have been explained. Heat capacity obtained from the density-of-states agrees with the experimental data up to 250 K at which the glass transition sets in and the experimental curve exhibits a marked change in slope.

Keywords: Polypropylene; Syndiotactic; Dispersion curves

1. Introduction

Polypropylene, an important fiber forming polymer, is known to exist in two tactic forms, i.e. isotactic and syndiotactic. Isotactic form has been well studied by Takeuchi et al. [1]. They have specially studied methyl torsion using inelastic neutron scattering and normal coordinate analysis. However, relatively less work have been done on the softer syndiotactic form. The syndiotactic form is known to crystallize in three different conformational states; helical form I, with *ggtt* as a repeat unit is the most common form [2–4], form II has an all *trans* sequence (*tttt*) [5], and form III conformationally ($t_2g_2t_6g_2$) assumes some of the conformational features of both forms I and II [6]. Here *g* and *t* denote *gauche* and *trans* conformational states, respectively, and the subscript stands for the number of such residues in a repeat unit.

The vibrational dynamics of syndiotactic polypropylene (sPP) of both forms I and II has been studied by several workers, e.g. Schactschneider and Snyder [7], Zerbi and Masetti [8] and others [7–10]. Most of this work is limited either by the use of approximate force field, lack of dispersion curves and their eventual use in obtaining thermodynamic parameters. Such infirmities seriously affect not only assignments but also the profile of dispersion curves, which in turn, affect density-of states and thermodynamic parameters such as heat capacity as a function of temperature. Recent studies [11] on thermal degradation of syndiotactic polypropylene show that the syndiotactic form is thermally more stable and more flexible as compared to the isotactic polypropylene. This is also supported by the relative magnitude of force constants.

In the present communication, we have accounted for all these infirmities by using Urey–Bradley force field (UBFF), which considers non-bonded interactions both in the gem- and tetra-configuration. The dispersion curves, density-of-states and heat capacity (10–460 K) thus obtained agree well with the Athas Data Update [12]. A comparative study of the isotactic and syndiotactic forms (forms I and II) is made to identify conformational sensitive modes and other spectral differences due to different orientation of the side group.

2. Theory

2.1. Calculation of normal mode frequencies

Normal mode calculation for a polymeric chain was

* Corresponding author. Tel.: +91 522 278 2653.
E-mail address: poonam_tandon@hotmail.com (P. Tandon).

0032-3861/$ - see front matter © 2005 Elsevier Ltd. All rights reserved.
doi:10.1016/j.polymer.2005.06.045

carried out using Wilson's GF matrix method [13] as modified by Higgs [14] for an infinite polymeric chain. The vibrational secular equation to be solved is

$$|G(\delta)F(\delta) - \lambda(\delta)I| = 0, \quad 0 \le \delta \le \pi \tag{1}$$

where δ is the phase difference between the modes of adjacent chemical units, $G(\delta)$ is the inverse kinetic energy matrix and $F(\delta)$ is the force field matrix for a certain phase value. The frequencies ν_i in cm^{-1} are related to eigen values by

$$\lambda_i(\delta) = 4\pi^2 c^2 \nu_i^2(\delta) \tag{2}$$

A plot of $\nu_i(\delta)$ versus δ gives the dispersion curve for the ith mode. The use of the type of force field is generally a matter of one's chemical experience and intuition [15]. In the present work we have used Urey–Bradley force field [16] Which has certain advantages over other fields such as valance force field etc. In the UBFF (1) relatively less parameters are required to express the potential energy, (2) no quadratic cross terms are included, the interaction between non-bonded atoms in gem- and tetra-configuration can be included and (3) the arbitrariness in choosing the force constants is reduced. Recently spectroscopically effective molecular mechanics models have been used for inter and intra molecular interactions consisting of charges, atomic dipoles and Vander Waals interactions [17].

2.2. Calculation of specific heat

Dispersion curves can be used to calculate the specific heat of a polymeric system. For a one-dimensional system the density of states function or the frequency distribution function expresses the way energy is distributed among the various braches of normal modes in the crystal, is calculated from the relation

$$g(\nu) = \sum \left[\left(\frac{\partial \nu_j}{\partial \delta} \right)^{-1} \right]_{\nu_j(\delta)=\nu_j} \tag{3}$$

The sum is over all the branches j. Considering a solid as an assembly of harmonic oscillators, the frequency distribution $g(\nu)$ is equivalent to a partition function. The constant volume heat capacity can be calculated using Debye's relation

$$C_\mathrm{v} = \sum g(\nu_j) K N_\mathrm{A} \left(\frac{h\nu_j}{KT} \right)^2 \left[\frac{\exp(h\nu_j/KT)}{\{\exp(h\nu_j/KT) - 1\}^2} \right] \tag{4}$$

with $\int g(\nu_i)\mathrm{d}\nu_i = 1$ the constant-volume heat capacity C_v, given by above equation, can be converted into constant-pressure heat capacity C_p using the Nernst–Lindemann approximation [18]:

$$C_\mathrm{p} - C_\mathrm{v} = 3RA_0 \frac{C_\mathrm{p}^2 T}{C_\mathrm{v} T_\mathrm{m}^0} \tag{5}$$

where A_0 is a constant often of a universal value [3.9×10^{-3} K mol/J] and T_m^0 is the estimated equilibrium melting temperature, which is taken to be 460.7 K [12].

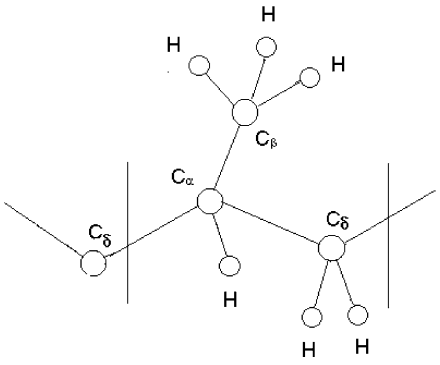

Fig. 1. One chemical repeat unit of sPP.

3. Results and discussion

A chemical repeat unit of sPP is shown in Fig. 1. The conformational repeat unit of sPP consists of two such chemical repeat units containing 18 atoms, which give rise to 54 dispersion curves. The frequencies of vibrations have been calculated for phase values ranging from 0 to π at an interval of .05π. Initially, force constants were transferred from syndiotactic poly (4-methyl, 1-pentene) [19] and then modified to obtain the 'best fit' to the observed infrared (FTIR) spectra [7]. The final force constants along with the internal coordinate are given in Table 1. Since the modes above 1350 cm^{-1} are non-dispersive in nature, dispersion curves are plotted in Figs. 2(a) and 3(a) for the modes below

Table 1
Internal coordinates and Urey–Bradley force constants (md/Å)

Internal coordinates	Force constants
$\nu[C_\beta–H]$	4.200
$\nu[C_\delta–H]$	4.150
$\nu[C_\alpha–H]$	4.360
$\nu[C_\alpha–C_\delta]$	3.300
$\nu[C_\alpha–C_\beta]$	3.700
$\varphi[H–C_\delta–H]$	0.390 (0.340)
$\varphi[H–C_\beta–H]$	0.405 (0.295)
$\varphi[C_\alpha–C_\delta–H]$	0.495 (0.255)
$\varphi[C_\delta–C_\alpha–H]$	0.540 (0.220)
$\varphi[C_\beta–C_\alpha–H]$	0.550 (0.210)
$\varphi[C_\alpha–,C_\beta–H]$	0.370 (0.200)
$\varphi[C_\alpha–C_\delta–C_\alpha]$	0.480 (0.175)
$\varphi[C_\delta–C_\alpha–C_\delta]$	0.500 (0.240)
$\varphi[C_\delta–C_\alpha–C_\beta]$	0.600 (0.220)
$\tau[C_\alpha–C_\delta]$	0.008
$\tau[C_\alpha–C_\beta]$	0.008
$\tau[C_\delta–C_\alpha]$	0.008
Off-diagonal interactions	
$\nu[C_\alpha–C_\delta] - \varphi[C_\alpha–C_\delta–H]$	0.300
$\nu[C_\alpha–C_\beta] - \varphi[C_\beta–C_\alpha–H]$	0.400

Note: ν, φ, ω, τ denote stretch, angle bend, wag and torsion, respectively. Stretching force constants between the non-bonded atoms in each angular triplet (gem configuration) are given in parentheses.

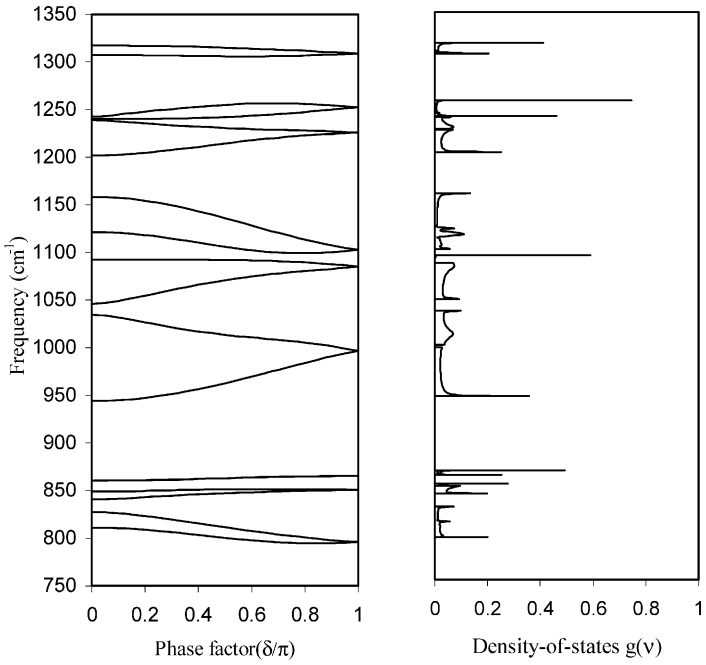

Fig. 2. (a) Dispersion curves of sPP (1350–750 cm^{-1}). (b) Density-of-states of sPP (1350–750 cm^{-1}).

1350 cm^{-1}. For the sake of simplicity, modes are discussed under two heads; non-dispersive and dispersive.

3.1. Non-dispersive modes

All modes above 1350 cm^{-1} are non-dispersive. The assignments of these modes are given in Table 2. The assignments have been made on the basis of potential energy distribution (PED), band shape, band intensity and appearance/disappearance of modes in similar molecules with atoms placed in similar environment. Spectra reported by Schactschneider and Snyder [7], Zerbi and Masetti [8], Tadokoro et al. [20] and Greggoriou et al. [21] for various tactic states of polypropylene have been made use of in the present studies.

The calculated frequencies in the C–H stretching region from 3100 to 2800 cm^{-1} are in good agreement with the observed bands. The region from 1380 to 1470 cm^{-1} contains bending modes of the methyl group and scissoring modes of the methylene group. The calculated frequencies in this region fit well with the observed data. The PED's shows that CH_3 symmetric bends mix with side chain C_α–C_β

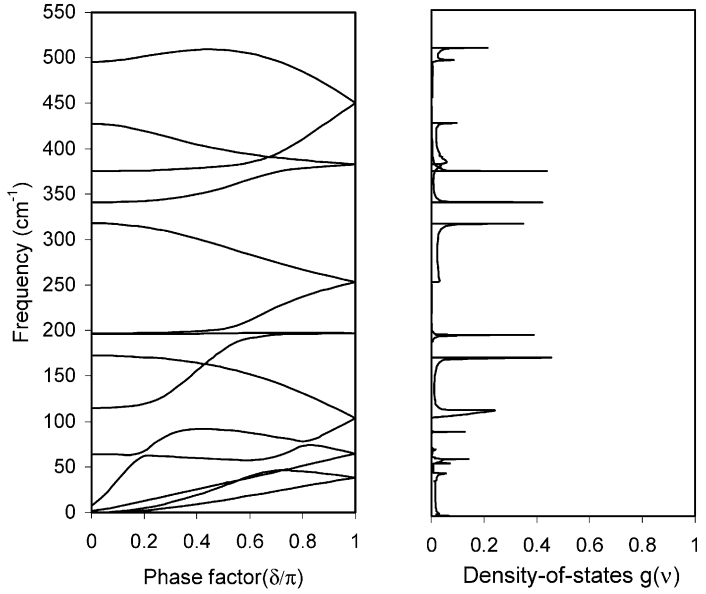

Fig. 3. (a) Dispersion curves of sPP below 550 cm^{-1}. (b) Density-of-states of sPP below 550 cm^{-1}.

Table 2
Non-dispersive modes of sPP

Frequency (cm^{-1})		Assignment (% PED) at $\delta=0$
Calc.	Observed (IR)[a]	
2959	2959	$\nu[C_\beta–H](99)$
2959	2959	$\nu[C_\beta–H](99)$
2928	2926	$\nu[C_\delta–H](79)+\nu[C_\alpha–H](20)$
2924	2926	$\nu[C_\delta–H](99)$
2917	2916	$\nu[C_\alpha–H](99)$
2914	2915	$\nu[C_\alpha–H](80)+\nu[C_\delta–H](19)$
2882	2880	$\nu[C_\beta–H](99)$
2882	2880	$\nu[C_\beta–H](100)$
2882	2880	$\nu[C_\beta–H](99)$
2882	2880	$\nu[C_\beta–H](99)$
2857	2856	$\nu[C_\delta–H](99)$
2857	2856	$\nu[C_\delta–H](99)$
1464	1466	$\varphi[H–C_\beta–H](95)$
1464	1466	$\varphi[H–C_\beta–H](94)$
1463	1466	$\varphi[H–C_\beta–H](95)$
1463	1466	$\varphi[H–C_\beta–H](94)$
1459	1455	$\varphi[H–C_\delta–H](74)+\varphi[C_\alpha–C_\delta–H](21)$
1456	1450	$\varphi[H–C_\delta–H](74)+\varphi[C_\alpha–C_\delta–H](18)$
1384	1381	$\varphi[H–C_\beta–H](36)+\varphi[C_\alpha–C_\beta–H](33)+\nu[C_\alpha–C_\beta](19)$
1381	1381	$\varphi[H–C_\beta–H](38)+\varphi[C_\alpha–C_\beta–H](35)+\nu[C_\alpha–C_\beta](21)$
1372	1372	$\varphi[C_\delta–C_\alpha–H](61)+\nu[C_\alpha–C_\delta](23)$
1357[b]	1350	$\varphi[C_\alpha–C_\delta–H](35)+\varphi[C_\beta–C_\alpha–H](26)+\varphi[C_\delta–C_\alpha–H](23)$
1317[b]	1322	$\varphi[C_\delta–C_\alpha–H](60)+\varphi[C_\alpha–C_\delta–H](14)+\nu[C_\alpha–C_\delta](12)$
1307	1322	$\varphi[C_\alpha–C–H](36)+\varphi[C_\beta–C_\alpha–H](22)+\varphi[C_\delta–C_\alpha–H](15)$
860[b]	867	$\varphi[C_\alpha–C_\beta–H](77)+\nu[C_\alpha–C_\delta](18)$
860	867	$\varphi[C_\alpha–C_\beta–H](78)+\nu[C_\alpha–C_\delta](12)$
849	841	$\varphi[C_\alpha–C_\beta–H](72)+\nu[C_\alpha–C_\delta](23)$
196	–	$\tau[C_\alpha–C_\beta](90)$

[a] Ref.[7].
[b] These modes are slightly dispersed.

stretch. The dispersion curves are essentially flat in this region. The bands in the region 1300–1370 cm^{-1} correspond to C_α–H bending and CH_2 wag modes. The C_α–H bend mode calculated at 1372 cm^{-1} and assigned to the peak at the same value has 23% contribution from backbone C_α–C_β stretch vibration. The other mode at 1307 cm^{-1} is mixture of C_α–H bend and CH_2 wag modes. Both these modes are non-dispersive.

Methyl rocking modes calculated at 860 and 849 cm^{-1} at $\delta=0$ are assigned to the observed peak at 867 cm^{-1}. These modes are mixed with side chain C_α–C_β stretch and are non-dispersive. A comparison of modes of planar sPP with helical sPP and iPP (Table 4) indicates that the non-dispersive modes are well localized and not much affected by change in configuration and conformation of PP chain.

3.2. Dispersive modes

The modes, which are dispersive, are mixed modes that are highly coupled along the chain. These modes are given in Table 3 at the zone center and zone boundary along with their assignments.

An interesting feature of the dispersive modes of sPP is their tendency to bunch towards the zone boundary. Such situation is also observed in other syndiotactic polymers [19]. It may arise when the PED of the two modes tends to overlap towards the zone boundary. In the observed spectra of sPP the 1233 cm^{-1} has been assigned to the planar all *trans* conformation of the backbone. Spectral studies on amorphous and crystalline samples show that its intensity increases with crystallinity. In our present calculation this mode is obtained at 1239 cm^{-1} at the zone center having a PED's of the CH_2 twist and C_α–H bending mode. In the planar form of syndiotactic polystyrene a skeletal mode is calculated and observed at 1221 cm^{-1} [22]. It may be inferred that this mode is characteristic of a planar backbone with syndiotactic side group attachments. The CH_2 twisting mode calculated at 1202 cm^{-1} at the zone center is assigned to the observed peak at 1200 cm^{-1}. The energy of this mode increases with increase in δ and C_α–H bending starts mixing. At the zone boundary this mode is calculated at 1226 cm^{-1} with large contribution coming from C_α–H bending. Both the above-mentioned twisting modes bunch and have same PED at the zone boundary. It is observed that the modes, which bunch in pairs, have some commonality in PED and hence appear to be strongly coupled. This

Table 3
All dispersive modes in sPP

Frequency (cm^{-1})		Assignment (%PED) at $\delta=0$	Frequency (cm^{-1})		Assignment (% PED) at $\delta=1$
Calc.	Observed (IR)[a]		Calc.	Observed (IR)[a]	
1243	–	$\varphi[C_\alpha–C_\delta–H](89)$	1252	–	$\varphi[C_\alpha–C_\delta–H](83)$
1240	1233	$\varphi[C_\alpha–C_\delta–H](36)+\varphi[C_\beta–C_\alpha–H](30)+\varphi[C_\delta–C_\alpha–H](22)$	1252	–	$\varphi[C_\alpha–C_\delta–H](83)$
1239	1233	$\varphi[C_\alpha–C_\delta–H](42)+\varphi[C_\beta–C_\alpha–H](29)$	1226	1233	$\varphi[C_\alpha–C_\delta–H](40)+\varphi[C_\beta–C_\alpha–H](31)+\varphi[C_\delta–C_\alpha–H](12)$
1202	1200	$\varphi[C_\alpha–C_\delta–H](99)$	1226	1233	$\varphi[C_\alpha–C_\delta–H](40)+\varphi[C_\beta–C_\alpha–H](31)+\varphi[C_\delta–C_\alpha–H](12)$
1158	1153	$\nu[C_\alpha–C_\delta](35)+\nu[C_\alpha–C_\beta](15)+\varphi[C_\delta–C_\alpha–C_\delta](10)$	1103	1095	$\nu[C_\alpha–C_\delta](36)+\nu[C_\alpha–C_\beta](22)+\varphi[C_\alpha–C_\delta–H](21)$
1121	1130	$\nu[C_\alpha–C_\beta](36)+\varphi[C_\alpha–C_\delta–H](28)+\nu[C_\alpha–C_\delta](12)$	1103	1095	$\nu[C_\alpha–C_\delta](36)+\nu[C_\alpha–C_\beta](22)+\varphi[C_\alpha–C_\delta–H](21)$
1093	1095	$\nu[C_\alpha–C_\delta](59)+\varphi[C_\delta–C_\alpha–H](17)$	1085	1095	$\nu[C_\alpha–C_\delta](56)+\varphi[C_\delta–C_\alpha–H](13)+\varphi[C_\alpha–C_\delta–H](10)$
1046	–	$\nu[C_\alpha–C_\delta](63)+\varphi[C_\alpha–C_\beta–H](17)+\varphi[C_\delta–C_\alpha–H](12)$	1085	1095	$\nu[C_\alpha–C_\delta](56)+\varphi[C_\delta–C_\alpha–H](13)+\varphi[C_\alpha–C_\delta–H](10)$
1035	–	$\nu[C_\alpha–C_\delta](60)+\varphi[C_\alpha–C_\delta–H](21)+\varphi[C_\alpha–C_\beta–H](10)$	997	972	$\varphi[C_\alpha–C_\delta–H](28)+\varphi[C_\alpha–C_\beta–H](22)+\nu[C_\alpha–C_\delta](20)$
944	962	$\varphi[C_\alpha–C_\beta–H](34)+\nu[C_\alpha–C_\beta](33)+\varphi C_\delta–C_\alpha–H](10)$	997	972	$\varphi[C_\alpha–C_\delta–H](28)+\varphi[C_\alpha–C_\beta–H](22)+\nu[C_\alpha–C_\delta](20)$
841	831	$\varphi[C_\alpha–C_\beta–H](59)+\nu[C_\alpha–C_\beta](18)+\nu[C_\alpha–C_\delta](11)$	851	831	$\varphi[C_\alpha–C_\beta–H](67)+\varphi[C_\alpha–C_\delta–H](19)$
827	828	$\varphi[C_\alpha–C_\delta–H](89)$	796	–	$\varphi[C_\alpha–C_\delta–H](41)+\nu[C_\alpha–C_\beta](29)+\nu[C_\alpha–C_\delta](16)$
811	–	$\varphi[C_\alpha–C_\delta–H](42)+\nu[C_\alpha–C_\beta](34)+\nu[C_\alpha–C_\delta](11)$	796	–	$\varphi[C_\alpha–C_\delta–H](41)+\nu[C_\alpha–C_\beta](29)+\nu[C_\alpha–C_\delta](16)$
495	492	$\varphi[C_\alpha–C_\delta–C_\alpha](45)+\varphi[C_\delta–C_\alpha–C_\beta](38)$	450	–	$\varphi[C_\delta–C_\alpha–C_\beta](35)+\varphi[C_\alpha–C_\delta–C_\alpha](19)+\varphi[C_\delta–C_\alpha–C_\delta](16)+\nu[C_\alpha–C_\delta](15)$
427	–	$\varphi[C_\delta–C_\alpha–C_\delta](34)+\varphi[C_\delta–C_\alpha–H](23)+\varphi[C_\beta–C_\alpha–H](14)+\varphi[C_\delta–C_\alpha–C_\beta](13)$	450	–	$\varphi[C_\delta–C_\alpha–C_\beta](35)+\varphi[C_\alpha–C_\delta–C_\alpha](19)+\varphi[C_\delta–C_\alpha–C_\delta](16)+\nu[C_\alpha–C_\delta](15)$
375	–	$\varphi[C_\delta–C_\alpha–C_\beta](56)+\varphi[C_\delta–C_\alpha–H](16)+\varphi[C_\beta–C_\alpha–H](12)$	383	–	$\varphi[C_\delta–C_\alpha–C_\beta](47)+\varphi[C_\delta–C_\alpha–H](16)+\varphi[C_\beta–C_\alpha–H](14)$
341	–	$\varphi[C_\delta–C_\alpha–C_\beta](80)$	383	–	$\varphi[C_\delta–C_\alpha–C_\beta](47)+\varphi[C_\delta–C_\alpha–H](16)+\varphi[C_\beta–C_\alpha–H](14)$
318	–	$\varphi[C_\delta–C_\alpha–C_\delta](43)+\varphi[C_\delta–C_\alpha–C_\beta](41)$	253	–	$\varphi[C_\delta–C_\alpha–C_\beta](51)+\varphi[C_\delta–C_\alpha–C_\delta](25)+\nu[C_\alpha–C_\delta](10)$
197	–	$\tau[C_\alpha–C_\beta](96)$	253	–	$\varphi[C_\delta–C_\alpha–C_\beta](51)+\varphi[C_\delta–C_\alpha–C_\delta](25)+\nu[C_\alpha–C_\delta](10)$
172	–	$\varphi[C_\delta–C_\alpha–C_\beta](47)+\varphi[C_\alpha–C_\delta–C_\alpha](35)$	197	–	$\tau[C_\alpha–C_\beta](97)$
115	–	$\tau[C_\alpha–C_\delta](49)+\tau[C_\delta–C_\alpha](39)$	103	–	$\varphi[C_\alpha–C_\delta–C_\alpha](44)+\varphi[C_\delta–C_\alpha–C_\delta](29)+\varphi[C_\delta–C_\alpha–C_\beta](10)$
64	–	$\tau[C_\delta–C_\alpha](51)+\tau[C_\alpha–C_\delta](44)$	103	–	$\varphi[C_\alpha–C_\delta–C_\alpha](44)+\varphi[C_\delta–C_\alpha–C_\delta](29)+\varphi[C_\delta–C_\alpha–C_\beta](10)$
0	–	$\nu[C_\alpha–C_\delta](38)+\varphi[C_\delta–C_\alpha–C_\delta](27)+\varphi[C_\alpha–C_\delta–C_\alpha](23)$	65	–	$\tau[C_\alpha–C_\delta](46)+\tau[C_\delta–C_\alpha](42)$
0	–	$\tau[C_\delta–C_\alpha](45)+\tau[C_\alpha–C_\delta](43)$	65	–	$\tau[C_\alpha–C_\delta](46)+\tau[C_\delta–C_\alpha](42)$
0	–	$\varphi[C_\alpha–C_\beta–H](50)+\varphi[H–C_\beta–H](46)$	38	–	$\tau[C_\delta–C_\alpha](49)+\tau[C_\alpha–C_\delta](45)$
0	–	$\varphi[C_\alpha–C_\beta–H](50)+\varphi[H–C_\beta–H](46)$	38	–	$\tau[C_\delta–C_\alpha](49)+\tau[C_\alpha–C_\delta](45)$

[a] Ref. [7].

commonality may be the result of strong intrachain interactions. This is true in case of polytetrafluroethylene [23], polystyrene [22] and poly(4-methyl, pentene 1) [19].

The modes calculated at 1158 and 1121 cm^{-1} at the zone center corresponding to the observed peak at 1153 and 1130 cm^{-1}, respectively, are coupled modes of C_α–C_β side chain and C_α–C_δ backbone stretches. With increase in δ the frequency and contribution of side chain C_α–C_β stretch increases in the former and decreases in the later. As in the case of CH_2 twisting modes, both these modes bunch at the zone boundary (calculated at 1103 cm^{-1} corresponding to the observed peak at 1095 cm^{-1}) and have same PED. The mode calculated at 1093 cm^{-1} is a mixed mode of backbone C_α–C_δ stretch and C_α–H bend at the zone center. The CH_3 rocking mode mixed with side chain C_α–C_β stretch is calculated at 944 cm^{-1} and assigned to the observed peak at 962 cm^{-1}.

The calculated frequency at 827 cm^{-1} with major contribution from CH_2 rocking matches well with the observed frequency at 828 cm^{-1}. This mode is observed at 832 cm^{-1} in planar sPP [24] and it is very sensitive to backbone conformation. It shifts to 812 cm^{-1} in helical sPP [10].

Comparison of the modes for sPP (all *trans*), sPP (helical) and iPP is shown in Table 4. The CH_2 wag, CH_3 rock and backbone C–C stretch and side chain C–C stretch, these three forms and skeletal deformation modes have large differences. These modes involve large coupling and are mixed with each other. The difference in the observed frequencies arises mainly because of the placement of the side group in different lateral positions, which in turn brings about the change in interaction constants, which are responsible for the frequency shifts. A greater change is expected in the low frequency region, but because of the

Table 4
Comparison of modes of sPP (all trans), sPP (helical) and iPP

Assignments	Frequency (cm^{-1})		
	sPP all trans observed (IR)	sPP helical observed (IR)	IPP observed (IR)
CH_3 asymmetric stretch	2959	2959	2956
CH_3 symmetric stretch	2880	2882	2880
CH stretch	2916, 2905	2915	2907
CH_2 asymmetric stretch	2926	2927	2925
CH_2symmetric stretch	2856[a]	2843	2868
CH_3 asymmetric deformation	1466	1465	1459
CH_2 scissoring	1455, 1450	1432, 1455	1454
CH_3 symmetric deformation	1381	1379	1377, 1359
CH_2 wag	1350	1287,1346	1378, 1305
CH_2 twist	1200, 1226	1234[b], 1202	1219, 1239
CH_2 rock	831, 829[b]	842, 812	841, 807
CH_3 rock	972, 867	977[b], 870	997, 973
CH bending	1322	1332	1329
C–C stretch (backbone)	1154, 1095	1153, 1035	1167, 1153
C–C stretch (sidechain)	1130	906, 1005[b]	1103, 1044
C–C–C bending	492	535, 483, 468	452

[a] Only calculated modes are known.
[b] Ref. [24].

non-availability of the spectra below 400 cm^{-1}, comparison is not possible. Although the spectra are not available below 400 cm^{-1}, calculations are expected to be correct for more than one reason. First, most of the frequencies occur in the same range as the corresponding ones in other synthetic polymers. Second, since the force constants, which provide good matching in the higher frequency region, are also involved in the lower frequency region, reasonable values are expected in this region as well.

3.3. Characteristic features of dispersion curves

The modes below 500 cm^{-1} have some special features like crossing repulsion etc. All such modes showing crossover in sPP are listed in Table 5 along with the PED and the δ values at which these features occur. To ascertain whether it is a crossing or a repulsion calculations at very close intervals of $\delta = .001\pi$ have been performed and it was found that the modes cross-over. From symmetry considerations, it can be shown that when the approaching modes belong to different symmetry species, they can cross over. Since sPP has mirror plane of symmetry along the chain axis, hence crossings are permissible [25]. Therefore, No two dispersion curves both of which belong to the same species can cross because this would imply the existence of two modes of vibrations with the same symmetry species and same frequency. This is also obvious from the Table 5 in which we have shown the pair of modes, which cross, belong to different symmetries, i.e. in plane and out-of-plane modes. In sPP crossing occurs for the pair of modes (115 and 172 cm^{-1}) and (375 and 427 cm^{-1}). Here we see that both the modes which crossover are dispersive. The intersection of acoustic modes at $\delta = .560\pi$ and $\delta = .741\pi$ can be regarded as an inelastic collision of two phonons in energy momentum space. Similar behavior is observed in poly(ε-capralactone) and poly(glycolic acid) [26,27].

In case of repulsion the two modes would exchange PED after repulsion. It does happen in case of dispersion curves which have zone center frequencies 7 and 64 cm^{-1} and repel at $\delta = .18\pi$. The PED of these modes exchange at this δ value. After repulsion these two modes diverges and again repelled at $\delta = .81\pi$. This interesting phenomenon of exchange of character may be viewed as a collision in the energy momentum space (ε, p) of two phonons approaching each other and moving apart after exchanging their PED.

3.4. Frequency distribution function and heat capacity

The frequency distribution function as obtained from dispersion curves is shown in Figs. 2(b) and 3(b). As explained in the theory section, the inverse of the slope of the dispersion curves leads to the density of states, which indicate how the energy is partitioned in various normal modes. The peaks in the frequency distribution curves compare well with the observed frequencies.

The frequency distribution function can also be used to calculate the thermodynamical properties such as heat capacity, enthalpy changes, etc. It has been used to obtain the heat capacity as a function of temperature. We have calculated the heat capacity of sPP in the temperature range 10–460 K using Debye's equation. The calculated heat capacity data is shown to be in good agreement with the experimental measurements (Fig. 4) as obtained from ATHAS data [12] when reduced to the results for a single monomeric residue per unit. However, deviation is seen above 305 K, which is the glass transition temperature. Above this temperature the amorphous regions present in a polymer pass on to rubbery state in which the different segments along the chain backbone acquire energy to rotate

Table 5
Pair of modes that cross

Frequency ($\delta=$)	$\delta^{\#}/\pi$	Before crossing			After crossing		
		δ^*/π	Frequency	PED	δ^*/π	Frequency	PED
i							
0	0.56	0.55	34	$\tau[C_\delta–C_\alpha](47)+\tau[C_\alpha–C_\delta](40)$	0.60	39	$\tau[C_\delta–C_\alpha](47)+\tau[C_\alpha–C_\delta](40)$
0	0.56	0.55	34	$\varphi[C_\alpha–C_\delta–C_\alpha](40)+\varphi[C_\delta–C_\alpha–C_\delta](34)$	0.60	38	$\varphi[C_\alpha–C_\delta–C_\alpha](37)+\varphi[C_\delta–C_\alpha–C_\delta](30)$
ii							
0	0.741	0.70	46	$\tau[C_\delta–C_\alpha](33)+\tau[C_\alpha–C_\delta](31)+\varphi[C_\alpha–C_\delta–C_\alpha](15)+\varphi[C_\delta–C_\alpha–C_\delta](11)$	0.75	48	$\tau[C_\delta–C_\alpha](43)+\tau[C_\alpha–C_\delta](39)$
0	0.741	0.70	44	$\tau[C_\delta–C_\alpha](45)+\tau[C_\alpha–C_\delta](46)$	0.75	46	$\tau[C_\delta–C_\alpha](44)+\tau[C_\alpha–C_\delta](46)$
iii							
115	0.43	0.40	164	$\varphi[C_\alpha–C_\delta–C_\alpha](40)+\varphi[C_\delta–C_\alpha–C_\beta](38)$	0.45	168	$\varphi[C_\alpha–C_\delta–C_\alpha](40)+\varphi[C_\delta–C_\alpha–C_\beta](38)$
172	0.43	0.40	155	$\nu[C_\alpha–C_\delta](26)+\varphi[C_\delta–C_\alpha–C](20)+\varphi[C_\alpha–C_\delta–C_\alpha](17)+\varphi[C_\delta–C_\alpha–C_\beta](10)$	0.45	162	$\nu[C_\alpha–C_\delta](26)+\varphi[C_\delta–C_\alpha–C_\delta](20)+\varphi[C_\alpha–C_\delta–C_\alpha](17)+\varphi[C_\delta–C_\alpha–C_\beta](10)$
iv							
375	0.675	0.65	392	$\varphi[C_\delta–C_\alpha–C_\beta](40)+\varphi[C_\delta–C_\alpha–H](18)+\varphi[C_\beta–C_\alpha–H](15)$	0.70	394	$\varphi[C_\delta–C_\alpha–C_\beta](41)+\varphi[C_\delta–C_\alpha–H](18)+\varphi[C_\beta–C_\alpha–H](15)$
427	0.675	0.65	388	$\varphi[C_\delta–C_\alpha–C_\beta](52)+\varphi[C_\delta–C_\alpha–H](10)$	0.70	390	$\varphi[C_\delta–C_\alpha–C_\beta](51)+\nu[C_\alpha–C_\delta](11)$

$\delta^{\#}$ corresponds to crossing/repulsion points. δ^* corresponds to the points before/after crossing/repulsion.

around the covalent bonds due to increased thermal energy. These segmental motions are not taken into account in the normal mode calculations and cause the deviation. The glass transition temperature depends on the side group present, intermolecular cohesive forces and the chain geometry, as these are sources of hindrances to the segmental mobility.

4. Conclusion

All characteristic features of the dispersion curves such as regions of high density-of-states, crossing over and repulsion have been well interpreted from the vibrational dynamics of syndiotactic polypropylene. A comparison is made with the spectra of its isotactic and helical form to identify the conformational sensitive modes. In addition the heat capacity as a function of temperature in the region 10–460 K has been successfully explained.

Acknowledgements

Financial assistance to one of the authors (PT) from the Council of Science and Technology, UP is gratefully acknowledged.

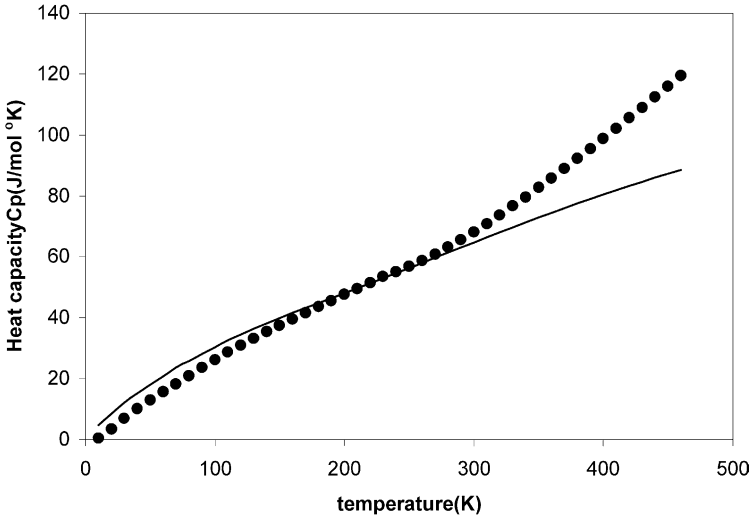

Fig. 4. Variation of heat capacity of sPP as a function of temperature. Solid line represents the theoretical values and (●) represents the experimental data.

References

[1] Takeuchi H, Higgins JS, Hill A, Mocanachi A, Allen G, Sterling GC. Polymer 1982;23.
[2] Cording P, Natta G, Ganis P, Temuussi PA. J Polym Sci Part C 1967; 16:2477.
[3] Rosa CD, Corradini P. Macromolecules 1993;26:5711.
[4] Auriemma F, Rosa CD, Corradini P. Macromolecules 1993;26:5719.
[5] Chatani Y, Maruyama H, Noguchi K, Asanuma T, Shiomura T. J Polym Sci Polym Lett 1990;28:393.
[6] Chatani Y, Maruyama H, Noguchi K, Asanuma T, Shiomura T. J Polym Sci Polym Phys Ed 1991;29:1649.
[7] Schachtschnisder JH, Snyder RG. Spectrochim Acta 1965;21:1527.
[8] Masetti G, Cabassi F, Zerbi G. Polymer 1980;21.
[9] Ishioka T, Masaoka N. Polymer 2002;43:4639.
[10] Hahn T, Suen W, Kang S, Hsu SL, Stidhou HD, Siedle AR. Polymer 2001;42:5813.
[11] Pang H, Xiao Y, Zhang P, Xing C, Zhu N, Zhu X, et al. Polym Degrad Stab 2005;88:473.
[12] ATHAS DATABANK 1993.
[13] Wilson EB, Decius JC, Cross PC. Moleculer vibrations: The theory of infrared and Raman vibrational spactra. New York: Dover Publications; 1980.
[14] Higgs PW. Proc Roy Soc (London) 1953;A220:472.
[15] Mannfors B, Palmo K, Krimm S. J Mol Struct 2000;556:1.
[16] Urey HC, Bradley HC. Phys Rev 1931;38:1969.
[17] Qian W, Mirikin NG, Krimm S. Chem Phys Lett 1999;315:125.
[18] Pan R, Verma-Nair M, Wunderlich B. J Therm Anal 1989;35:955.
[19] Pande S, Kumar A, Tandon P, Gupta VD. Vibr Spectrosc 2001;26:161.
[20] Tadokaro H, Kobayashi M, Ukita M, Yasupuku K, Murahashi S. J Chem Phys 1965;42:4.
[21] Gregoriou V, Kandilioti G, Gatos KG. Vibr Spectrosc 2004;34:47–53.
[22] Rastogi S, Gupta VD. J Macromol Sci 1994;B33(2):129.
[23] Hannon MJ, Boerio FJ, Koenig JL. J Chem Phys 1969;50:2829.
[24] Nakaoki T, Yamanaka T, Ohira Y, Horii F. Macromolecules 2000;33: 2718.
[25] Bower DI, Maddams WF. The vibrational spectroscopy of polymers. Cambridge: Cambridge University Press; 1989.
[26] Misra RM, Agarwal R, Tandon P, Gupta VD. Eur Polym J 2004;40: 1787.
[27] Agarwal R, Misra RM, Tandon P, Gupta VD. Polymer 2004;45:5307.